A fully reconfigurable photonic integrated signal processor

Weilin Liu,[1†] Ming Li,[1†] Robert S. Guzzon,[2†] Erik J. Norberg,[2] John S. Parker,[2] Mingzhi Lu,[2] Larry A. Coldren,[2] and Jianping Yao[1]*

[1]Microwave Photonics Research Laboratory, University of Ottawa, Ottawa, Ontario K1N 6N5, Canada
[2]Department of Electrical and Computer Engineering, University of California Santa Barbara, Santa Barbara, California 93116, USA
†These authors contributed equally to this work.

*To whom correspondence should be addressed; E-mail: jpyao@eecs.uottawa.ca.

Photonic signal processing has been considered a solution to overcome the inherent electronic speed limitations (1-3). Over the last few years, an impressive range of photonic integrated signal processors have been proposed (1-6), but they mainly offer limited reconfigurability, a feature highly needed for the implementation of large-scale general-purpose photonic signal processors. Here we report and experimentally demonstrate a fully reconfigurable photonic integrated signal processor based on an InP-InGaAsP material system. The proposed photonic signal processor is capable of performing reconfigurable signal processing functions including temporal integration, temporal differentiation, and Hilbert transformation. The reconfigurability is achieved by controlling the injection currents to the active components in the signal processor. Our demonstration suggests high potential for chip-scale fully programmable all-optical signal processing.

One of the fundamental challenges for digital signal processing (DSP) is the limited speed which is mainly restricted by the electronic sampling rate. In an optical network, signal processing is implemented based on DSP, which involves electronic sampling, optical-to-electronic (OE) and electronic-to-optical (EO) conversions. A solution to achieve power-efficient and high-speed signal processing in an optical network is to implement signal processing directly in the optical domain using a photonic signal processor to avoid the need of electronic sampling, OE and EO conversions (1-3). To date, numerous photonic signal processors have been reported based on either discrete components or photonic integrated circuits (1-10). A photonic signal processor based on discrete components usually has decent programming abilities but it is usually more bulky and less power efficient, while a photonic integrated signal processor has a much smaller footprint and higher power efficiency. A photonic signal processor can be used to implement fundamental signal generation and processing functions such as optical pulse shaping and arbitrary

waveform generation (1), optical dispersion compensation (7), temporal integration (8), temporal differentiation (9), and Hilbert transformation (10). These functions are basic building blocks of a general-purpose signal processor for signal generation and fast computing. Fast computing such as temporal integration, temporal differentiation, and Hilbert transformation can find important applications (11-23). For example, a photonic integrator is a device that is able to perform time integral of an optical signal, which can find applications in dark soliton generation (12), optical memory (13), and optical analog-to-digital conversion (14). One of the most important characteristic parameters of a photonic integrator is the integration time. A long integration time means a better integration capability. An ideal photonic temporal integrator should have an infinite integration time. An on-chip CMOS-compatible all-optical integrator based on an add-drop ring resonator with an integration time of 800 ps was reported (15). For many applications, however, an integration time as long as a few nanoseconds is needed. To achieve such a long integration time, the insertion loss must be precisely compensated to obtain an high *Q*-factor, which is very challenging especially for a stable operation without causing lasing. In addition, an integrator with a fractional or higher order is also needed, which is more difficult to implement (16). A photonic temporal differentiator (17) is a device that performs temporal differentiation of an optical signal, which can find applications such as all-optical Fourier transform (18, 19), temporal pulse characterization (20), and optical TDM (OTDM) demultiplexing (21). A photonic Hilbert transformer is a device that derives the analytic representation of a signal (22), and has been widely used for single-sideband (SSB) modulation. SSB modulation is particularly useful in a radio-over-fiber (RoF) link to avoid dispersion-induced power fading (23). Although the photonic implementations of these functions have been reported (8, 9, 10, 15, 17, 22), a signal processor is usually designed to perform a specific function with no or very limited reconfigurability. For general-purpose signal processing, however, a photonic signal processor should be able to perform multiple functions with high reconfigurability.

In this paper, we report the design, fabrication and experimental demonstration of a fully reconfigurable photonic integrated signal processor, to perform the above-mentioned three signal processing functions. The photonic signal processor consists of three active microring resonators (R1, R2, and R3) and a bypass waveguide as a processing unit cell, as shown in Fig. 1(a) and Fig. 1(b). To obtain on-chip reconfigurability, we incorporate nine semiconductor optical amplifiers (SOAs) and twelve current-injection phase

modulators (PMs) in the unit cell, as shown in Fig. 1(b). The tunable coupling between two neighboring rings and between the outer ring and the bypass waveguide is realized using four tunable couplers (TCs) with each consisting of two multi-mode interference (MMI) couplers and two PMs, as shown in the inset in Fig. 1(b). The coupling ratio in each TC can be tuned by adjusting the injection currents to the two PMs in the TC. Within each ring, there are two SOAs used to compensate for the waveguide propagation loss, and the MMI splitting loss and insertion loss. When an SOA is forward biased, it can create an optical gain. On the other hand, an SOA can operate as an optical absorber when it is reverse biased, which is the key to achieve the configurability of the processor. Consequently, with the SOAs utilized in this design, a waveguide path could effectively be on or off to facilitate the synthesis of various circuit geometries. By reverse biasing one SOA in each of the three ring resonators, for example, the three mutually coupled rings are reduced to a single optical path. With the bypass waveguide incorporated in the design, the chip can be reconfigured as a Mach-Zehnder interferometer (MZI). The signal processing functions including temporal integration, temporal differentiation, and Hilbert transformation can be implemented by configuring the unit cell with a specific geometry. In addition, there is a current-injection PM in each ring resonator, and a PM in the bypass waveguide, which are used to achieve wavelength tunability. Furthermore, the order of the signal processor, either a fractional or higher order, can be tuned by tuning the coupling ratio of the TC. The actually fabricated device is shown in Fig. 1(c), which is wire-bonded to a carrier to enable an easily access to the SOAs and PMs with the assistance of a customized probe station. In the following, the proposed integrated photonic signal processor reconfigured to achieve three different functions for fast signal processing is discussed.

Photonic temporal integrator

An *n*th-order temporal integrator is a linear time-invariant (LTI) system with a transfer function given by (16)

$$H_n(\omega) = \left[\frac{1}{j(\omega - \omega_0)}\right]^n \tag{1}$$

where $j=\sqrt{-1}$, ω is the optical angular frequency and ω_0 is the carrier frequency of the signal to be processed. A first-order photonic temporal integrator can be implemented using an optical resonator, for example, an add-drop ring resonator (16). If the input and drop ports are used, the ring resonator would have a spectral response that is close to that given in (eq. 1) for n = 1, and it is a first-order temporal integrator. A higher-order (with n = 2, 3, …) temporal integrator can be implemented by cascading or coupling n first-order integrators (16). An nth-order temporal integrator is capable of calculating the nth time integral of an arbitrary optical waveform.

The photonic integrated signal processor shown in Fig. 1 can be configured as a temporal integrator with an order of 1, 2 and 3, depending on the number of rings used. In the unit cell, there are three mutually coupled ring resonators with two active SOAs in each ring resonator. If one SOA in a ring resonator is reverse biased to shut off the waveguide, the ring resonator simply becomes a waveguide. By controlling the number of rings in the unit cell to be 1, 2 or 3, a temporal integrator with an order of 1, 2 or 3 is achieved. For example, a temporal integrator with an order of 1 is configured by shutting off two ring resonators, as shown in Fig. 2(a). In each ring resonator, a current injection PM is incorporated, which is used to tune the resonance frequency of the ring resonator, thus achieving wavelength tunability. In addition, the tunable coupling between two adjacent rings, and between an outer ring (R1 or R3) and the bypass waveguide, can offer tunable spectral response of the coupled-ring resonator, which can be used to achieve higher order integrators.

Photonic temporal differentiator

An nth-order temporal differentiator provides the nth order time derivative of the envelope of an optical signal. An nth-order temporal differentiator can be considered as an LTI system with a transfer function given by

$$H_n(\omega)=\left[j(\omega-\omega_0)\right]^n=\begin{cases}e^{jn\frac{\pi}{2}}|\omega-\omega_0|^n & \omega>\omega_0\\ e^{-jn\frac{\pi}{2}}|\omega-\omega_0|^n & \omega<\omega_0\end{cases} \quad (2)$$

As can be seen an *n*th-order temporal differentiator has a magnitude response of $|\omega-\omega_0|^n$ and a phase jump of $n\pi$ at ω_0. An optical filter with a frequency response given by (eq. 2) can be implemented using an MZI (24). By controlling the coupling coefficients of the input and output couplers in an MZI, a tunable phase shift from 0 to 2π can be achieved, thus a temporal differentiator with a tunable fractional order can be implemented. The photonic integrated signal processor shown in Fig. 1 can be configured to have an MZI structure as shown in Fig. 3(a). One arm of the MZI is formed by shutting off the three ring resonators in the unit cell, by applying a reverse bias to one of the two SOAs in each of the three ring resonators. The other arm is the bypass waveguide. The tuning of the fractional order is achieved by changing the coupling coefficients at both the input and output couplers. The operation wavelength can also be tuned, which is done by tuning the injection current applied to the PM in one of the MZI arms.

Photonic temporal Hilbert transformer

A *n*th order Hilbert transformer is an LTI system with a transfer function given by (25)

$$H_n(\omega)=\begin{cases} e^{-jn\frac{\pi}{2}} & \omega>0 \\ e^{jn\frac{\pi}{2}} & \omega<0 \end{cases} \tag{3}$$

As can be seen an *n*th-order Hilbert transformer has a magnitude response of 1 and a phase jump of $n\pi$ at ω_0. A fractional Hilbert transformer becomes a conventional Hilbert transformer when $n = 1$. For $n = 0$, we have $H_0(\omega)=1$, which is an all-pass filter. For $0 < n < 1$, the output is a weighted sum of the input signal and its conventionally Hilbert transformed signal (25). In addition, a fractional Hilbert transformer with an order of n is equivalent to two cascaded fractional Hilbert transformers with fractional orders of α and β if $\alpha+\beta = n$. A ring resonator can be used to implement a Hilbert transformer if the *Q*-factor is high. For a ring resonator with a high *Q*-factor, the spectral response is close to all pass, except a narrow notch, which is small enough and would contribute negligible error to the transform (26). Fig. 4(a) shows the configuration. Although the three ring resonators in the processor can be independently enabled or disabled, they are coupled in series. As a result, only one fractional Hilbert transformer or two cascaded fractional Hilbert

transformers can be configured in the unit cell corresponding to a single-ring or two-cascaded-ring structure with all-pass configuration.

Results

The proposed signal processor is fabricated in an InP-InGaAsP material system, which is wire-bonded to a carrier for experimental demonstration, as shown in Fig. 1(c). The SOAs in each ring are measured to have a peak gain of 9.6 dB per SOA, which can be used to compensate for the insertion loss or to shut off the ring. The coupling coefficients of the TCs are measured at different injection currents to the PMs, which can be controlled from 0 to 100% when one of the PMs in each of the TCs is injected with a current from 0 to 3.5 mA. There are twenty-one active components (SOAs and PMs) in a unit cell. When injection currents are applied, they will generate heat, which will shift the resonance wavelengths of the ring resonators and degrade the system stability. In the experiment, the chip is temperature controlled by a temperature control unit to ensure the working temperature is 22^{o}C, to maintain a stable operation.

Integrator: We first test the operation of the photonic temporal integrator with an order of $n = 1$. As a first-order integrator, the photonic integrated signal processor is configured to operate as a single ring resonator (R1 is on, R2 and R3 are off), as shown in Fig. 2(a), where the output optical signal is converted to an electrical signal at a photodetector and monitored by an oscilloscope. The free spectral range (FSR) is measured by an optical vector analyzer (OVA, Luna) to be 0.22 nm, as shown in Fig. 2(b). By changing the injection current to the PM in the ring (the PM in R1), the spectral response of the ring is laterally shifted, thus the peak location is also shifted, as shown in Fig. 2(c), which confirms the tuning of the working wavelength. In the experiment, an optical Gaussian pulse generated by a mode-locked laser (MLL) source and spectrally shaped by an optical bandpass filter (Finisar, WaveShaper 4000S) with a full width at half maximum (FWHM) of 46 ps centered at 1557.4 nm, as shown as the red curve in Fig. 2(b) and the inset in Fig. 2(d), is then coupled into the temporal integrator via a lensed fiber. Fig. 2(d) shows the first-order temporal integral of the input Gaussian pulse. The integration time is measured to be 10.9 ns, which is more than one order of magnitude longer than the result reported in (15). With a rising time of 48 ps, the proposed photonic integrator offers a time-bandwidth product (15) (TBWP, a principal figure of merit, represents the throughput limit for an optical system determined by the product of the bandwidth and the

time-bandwidth of the optical system) of 227, which is much higher than an advanced electronic integrator (TBWP<10) (27), and also more than two-times greater than the previously reported photonic integrator (TBWP~100) (15). The *Q*-factor is also calculated based on the integration time, which is ~50 million.

Then, the photonic integrated signal processor is configured as a second-order (where R1 and R2 are on and R3 is off), and a third-order (where R1, R2 and R3 are all on) temporal integrator with two and three coupled ring resonators on the chip. The integration of the input Gaussian pulse at the outputs of the second- and third-order temporal integrator is then obtained, which are shown in Fig. 2(e). A higher order integrator, such as a second- and third-order integrator, can be used, for example, to solve higher order ordinary differential equations (15, 16). A second-order integrator can also be used for arbitrary waveform generation (11). The first-order integral of an in-phase and out-of-phase doublet pulse is also computed by the proposed first-order temporal integrator. An in-phase/out-of-phase doublet consists of two temporally separated in-phase/out-of-phase Gaussian waveforms with identical amplitude profile. As shown in Fig. 2(f) and (g), the temporal integrator sums up the area under the two field amplitude waveforms for the case of in-phase doublet pulse. Since the phase relationship between the two pulses of the in-phase doublet is not maintained during multiple round-trips in the ring resonator due to the dynamic intensity-dependent refractive index variations, the magnitude of the integration output is not well maintained, which leads to a reduced integration time of 7.8 ns. For the case of out-of-phase doublet pulse, the time integral of the second waveform in the doublet pulse cancels that of the first waveform, leading to a square-like profile with the duration determined by the time delay between the two waveforms of the doublet pulse. As shown in Fig. 2(g), the two out-of-phase pulses do not subtract completely, this is because the two pulses are not perfectly identical in amplitude and phase due to a slight asymmetry of the MZI used to generate the two pulses (the two pulses are generated by splitting a single pulse to two pulses and recombining the time-delayed pulses at the output of the MZI). These results suggest important applications of a photonic integrator as a memory unit, such as “write” and “erase” operations (15). Simulations are also performed to calculate the temporal integral of the input pulse and the results are plotted with dashed line as shown in Fig. 2(d)-(g). As can be seen, the experimental results agree well with the simulation results. The active components such as the SOAs and PMs in the processor offer a precise control of the resonance peak and the *Q*-factor of each ring resonator, which is indispensable for achieving higher order integration (8). This

is the first time that a higher order (up to 3) photonic temporal integrator is implemented on an integrated chip.

Differentiator: The photonic integrated signal processor is then configured to have an MZI structure to implement a fractional order temporal differentiator (where R1, R2 and R3 are all off, forming one arm of the MZI, the bypass waveguide forms another arm of the MZI), as shown in Fig. 3(a). Again, a photodetector is connected at the output of the chip to convert the optical signal to an electrical signal. The spectral response of the MZI is shown in Fig. 3(b). It has an FSR of 0.44 nm. By changing the injection current to the PM in one of the two arms, the spectral response is then laterally shifted, as shown in Fig. 3(b). By changing the injection current to the PMs in the tunable couplers at the input or output of the MZI, the coupling coefficient can be tuned to achieve tunable phase shift at the transmission notch. Fig. 3(c) and (d) shows the measured transmission notch with a phase jump from 0 to π by an optical vector network analyzer (OVA, Luna). A Gaussian pulse with a temporal width of 33 ps centered at 1558.7 nm, shown in Fig. 3(c) and (e), is coupled into the chip. Five differentiated pulses corresponding to five differentiation orders of 0.785, 0.842, 1, 1.2, and 1.68 are obtained, which are shown in Fig. 3(f) to (j), respectively. The phase information of the differentiated pulses is also shown. Again, simulations are also performed to calculate the temporal differentiation of the input Gaussian pulse with five differentiation orders of 0.785, 0.842, 1, 1.2, and 1.68. The results are also shown in Fig. 3(f)-(j). As can be seen, the experimental results agree well with the simulation results. The slightly mismatch in the dip between the simulation and experimental output waveforms is due to the limited bandwidth of the photodetector. The proposed differentiator can provide an analog processing bandwidth of 55 GHz, as can be seen from Fig. 4(c), which is significant larger than an electronic microwave differentiator (28). With such a large bandwidth, the photonic differentiator can provide fast signal processing and signal coding (24). In addition, the differentiation order is also tunable, which provides better flexibility in signal processing, such as tunable image enhancement (29).

Hilbert transformer: The photonic integrated signal processor can also be configured to have a single ring or two cascaded ring structure to implement a fractional Hilbert transformer or two cascaded fractional Hilbert transformers. Fig. 4(a) shows the configuration as a single-ring fractional Hilbert transformer (R1 is

on, R2 and R2 are off). The spectral response of the single-ring fractional Hilbert transformer is measured and shown in Fig. 4(b) with an FSR of 0.22 nm. By changing the injection current to the PM in the ring, the notch location is tuned and the FSR is slightly changed as shown in Fig. 4(b). The phase response which determines the fractional order of the Hilbert transform can also be tuned by changing the coupling coefficient between the ring and the bypass waveguide, as shown in Fig. 4(c) and (d), which is achieved by changing the injection current to the PMs in the TCs. To validate the operation of the processor as a fractional Hilbert transformer, an optical Gaussian pulse with a central wavelength at 1559.1 nm and a temporal width of 33 ps, shown in Fig. 4(e), is coupled into the chip. The fractional order of the Hilbert transformer is continuously tunable from 0 to 1 by changing the coupling coefficient through controlling the injection currents to the PMs in the TC. Fig. 4(f), (g), and (h) shows the fractionally Hilbert transformed pulses with a tunable fractional order from 0.5 to 1. The fractional order Hilbert transformer can be used to construct a secure communication system (25), in which the fractional order *n* is used as a secret key for demodulation. If the order *n* is unknown in the demodulation, the signal cannot be recovered. The proposed fractional order Hilbert transformer can also provide fast tunability of the fractional order, which can be used in secure communications with dynamic secrets.

The signal processor can also be configured as two cascaded Hilbert transformers (R1 and R3 are on, and R2 is off). Fig. 4(h) and (i) shows the output pulses with the fractional orders of (1.0, 0.25) and (1.0, 1.0) which are equivalent to a single Hilbert transformer with a fractional order of 1.25 and 2. Again, the tuning is achieved by changing the coupling coefficients through controlling the injection currents to the PMs in the tunable couplers. Comparing to the most recently reported tunable fractional Hilbert transformer in a chip-scale device (22), the proposed Hilbert transformer offers a much easier control of the tunable fractional order through tuning the injection current instead of changing the polarization states of the input signal.

The proposed photonic signal processor can be reconfigured as a photonic temporal integrator, differentiator, and Hilbert transformer, which are basic building blocks for general-purpose signal processing. The proposed photonic signal processor can be used to provide high-speed processing to break the speed and bandwidth bottleneck of an electronic processor. For example, a photonic temporal integrator

is one of the most important components in a delta-sigma converter for optical analog to digital conversion (14). A photonic temporal differentiator can be used in demultiplexing an OTDM signal (21) and performing real-time amplitude and phase measurement of an optical signal. A Hilbert transformer can be used to generate a wideband SSB modulated signal, which is useful in a radio-over-fiber (RoF) link to avoid dispersion-induced power penalty (23). If the designed photonic signal processor is employed in an optical network, the above-mentioned functionalities can be achieved with a single integrated photonic chip. More importantly, with the development of all-optical networks, photonic signal processors can be incorporated into an optical network to perform fast signal processing without digital sampling, and OE and EO conversions. Thus, the proposed photonic signal processor can provide a potential cost-effective solution for signal processing in future all-optical networks.

In real applications, the proposed high speed processor should be able to provide accurate signal processing with small errors. To evaluate the error performance, an error analysis is performed using the measured transfer functions of the photonic signal processor that is reconfigured as an integrator, a differentiator, and a Hilbert transformer. We assume that the input pulse is an ideal Gaussian pulse and the absolute errors are calculated as the difference between the intensities of the simulated output waveform based on the measured transfer functions and the numerically calculated waveform. Since an ideal integrator has a temporal output extending to infinity if the input is a Gaussian pulse, and our proposed integrator can provide a finite integration time of 10.9 ns, the errors in the analysis are measured in a time duration of 20 ns. The mean absolute errors of the processor to perform each of the functions can be found in Fig. 5. As can be seen, the integrator, differentiator, and Hilbert transformer can operate with a minimum error for an input Gaussian pulse with a bandwidth of 19.11, 19.72, and 30.84 GHz, respectively. The proposed photonic signal processor can work for a pulse with a different bandwidth, at the cost of increased mean absolute errors. The processing of a rectangular pulse sequence as an input signal is also evaluated. For example, for a rectangular pulse sequence the Hilbert transformer has an optimal processing bandwidth of 30.84 GHz. A binary rectangular pulse sequence with a duty cycle of 50% and a period of 57 ps can be processed with a minimum error, which corresponds to a data rate of 17.5 Gbps. If a multilevel signal is used, the data rate can be higher.

Discussion and Summary

In the experiment, the power of the input optical pulses is below -10 dBm, and the SOAs inside the ring resonators are working with small injection currents to provide small gain to compensate for the insertion losses, thus the nonlinear effects in the rings are small and negligible. However, nonlinear effects such as self-phase modulation and four-wave mixing have to be considered if the power of the input signal is high. To utilize the proposed processing unit cell in a large system, the power consumptions of the PMs and SOAs, and the amplified spontaneous emission (ASE) noise from the SOAs should be also considered. In the experiment, for example, the total power consumption of the first-order integrator is 350 mW including 148 mW consumed by the input/output SOAs, which can be significantly reduced in a large system where all units are fabricated on a single chip without fiber coupling loss between the units. In addition, the SOAs have a length of 400 μm, therefore, the SOAs in the ring resonators only operate at a low current density. This low-current-density operation increases the ASE noise. A potential solution to reduce the ASE noise and further increase the integration time is to use SOAs with shorter lengths, thus the SOAs can operate at a much higher operation current density. Operating at a high current density, a single SOA is sufficient to compensate for the insertion loss inside each ring resonator, therefore, the number of SOAs can also be reduced for large scale integration, and the power consumption is reduced. As can be seen from Fig. 2(b), Fig. 3(b), and Fig. 4(b), the bandwidth of the proposed photonic signal processor when reconfigured as an integrator and a Hilbert transformer is 27 GHz or 0.22 nm at 1550 nm, limited by the FSR of the ring resonators. When reconfigured as a differentiator, the bandwidth is 55 GHz or 0.44 nm at 1550 nm, limited by the FSR of the MZI. A shortened length of the ring resonators will lead to a greater FSR and further increase the bandwidth of the signal processor.

Since the reconfigurability and tunability of the proposed photonic signal processor are achieved by tuning the injection currents to the active components (nine SOAs and twelve PMs) on the chip, the processor needs twenty-one current injection sources to realize full system reconfigurability and wavelength tunability. In the experiment, the SOAs and PMs on the chip are controlled by adjusting the injection currents from multiple source measurement units (SMUs). Those SMUs, for practical applications, can be replaced by a customized electronic unit with programmable current control, such as a field-programmable

gate array (FPGA). By programming the FPGA, the signal processor can be reconfigured for different signal processing functions. In the proposed photonic signal processor, a stable resonance wavelength and a high *Q*-factor are critical for achieving a long integration time. However, the ambient temperature change can shift the resonance wavelength of the ring resonators and change the gain profiles of the SOAs, which will alter the working wavelengths and decrease the *Q*-factors of the ring resonators. To maintain a stable temperature in the signal processor for good stability, a TEC is added in the electronic unit to improve the stability, and thus to increase the integration time.

In summary, we have designed, fabricated and demonstrated a fully reconfigurable photonic integrated signal processor based on a photonic integrated circuit. The operation of the signal processor reconfigured as a temporal integrator, a temporal differentiator and a Hilbert transformer with a tunable order and a tunable operation wavelength was demonstrated experimentally. In particular, a temporal integrator over a bandwidth of 0.22 nm with an integration time of 10.9 ns was achieved, which is the longest integration time ever reported. Although some photonic signal processing functions, such as arbitrary waveform generation and optical dispersion compensation, are not implemented with the current design, this work represents an important step towards the realization of a fully programmable high speed and wideband general-purpose photonic signal processors that can overcome the inherent speed limitation of electronic signal processors.

References and Notes:

[1] M. Kahn , H. Shen , Y. Xuan , L. Zhao , S. Xiao , D. Leaird , A. Weiner, and M. Qi, "Ultrabroad-bandwidth arbitrary radiofrequency waveform generation with a silicon photonic chip-based spectral shaper," *Nature Photon.*, vol. 4, no. 2, pp.117-122, Feb. 2010.

[2] R. Yu, S. Cheung, Y. Li, K. Okamoto, R. Proietti, Y. Yin, and S. J. B. Yoo, "A scalable silicon photonic chip-scale optical switch for high performance computing systems," *Opt. Express*, vol. 21, no. 26, pp. 32655-32667, Dec. 2013.

[3] A. E. Willner, S. Khaleghi, M. R.Chitgarha, and O. F. Yilmaz, "All-optical signal processing," *J. Lightwave Technol.*, vol. 32, no. 4, pp. 660-680, Feb. 2014.

[4] C. Koos , P. Vorreau, T. Vallaitis , P. Dumon, W. Bogaerts, R. Baets, B. Esembeson, I. Biaggio, T. Michinobu, F. Diederich, W. Freude, and J. Leuthold, "All-optical high-speed signal processing with silicon-organic hybrid slot waveguides," *Nat. Photonics*, vol. 3, no. 4, pp. 216-219, Apr. 2009.

[5] A. M. Weiner, "Ultrafast optical pulse shaping: A tutorial review," *Opt. Commun.*, vol. 284, no. 15, pp. 3669–3692, Jul. 2011.

[6] V. R. Almeida, C. A. Barrios, R. Panepucci, and M. Lipson, "All-optical control of light on a silicon chip," *Nature*, vol. 431, no. 7012, pp. 1081–1084, Oct. 2004.

[7] C. R. Doerr and K. Okamoto, "Advances in silica planar lightwave circuits," *J. Lightwave Technol.*, vol. 24, no. 12, pp. 4763-4789, Dec. 2006.

[8] R. Slavík, Y. Park, N. Ayotte, S. Doucet, T. Ahn, S. LaRochelle, and J. Azaña, "Photonic temporal integrator for all-optical computing," *Opt. Express*, vol. 16, no. 22, pp. 18202-18214, Oct. 2008.

[9] N. Q. Ngo, S. F. Yu, S. C. Tjin, and C. H. Kam, "A new theoretical basis of higher-derivative optical differentiators," *Opt. Comm.*, vol. 230, no. 1-3, pp. 115-129, Jan. 2004.

[10] H. Shahoei, P. Dumais, and J. P. Yao, "Continuously tunable photonic fractional Hilbert transformer using a high-contrast Germanium-doped silica-on-silicon microring resonator," *Opt. Lett.*, vol. 39, no. 9, pp. 2778-2781, May 2014.

[11] R. Ashrafi, M. R. Dizaji, L. R. Cortés,J. Zhang, J. P. Yao, J. Azaña, and L. R. Chen, "Time-delay to intensity mapping based on a second-order optical integrator: application to optical arbitrary waveform generation," *Opt. Express*, vol. 23, no. 12, pp. 16209-16223, Jun. 2015.

[12] N. Q. Ngo and L. N. Binh, "Optical realization of Newton-Cotes-based integrators for dark soliton generation," *J. Lightw. Technol.*, vol. 24, no. 1, pp. 563-572, Jan. 2006.

[13] M. T. Hill, H. J. S. Dorren, T. de Vries, X. J. M. Leijtens, J. H. den Besten, B. Smallbrugge, S. Oei, J. J. M. Binsma, G. D. Khoe, and M. K. Smit, "A fast low power optical memory based on coupled micro-ring lasers," *Nature*, vol. 432, no. 7014, pp. 206–209, Nov. 2004.

[14] E. Reeves, P. Costanzo-Caso, and A. Siahmakoun, "Theoretical study and demonstration of photonic asynchronous first-order delta-sigma modulator for converting analog input to NRZ binary output," *Microw. Opt. Technol. Lett.*, vol. 57, no. 3, pp. 574-578, Mar. 2015.

[15] M. Ferrera, Y. Park, L. Razzari, B. E. Little, S. T. Chu, R. Morandotti, D. J. Moss, and J. Azaña, "On-chip CMOS-compatible all-optical integrator," *Nature Commun.*, vol. 1, no. 29, pp. 1-5, Jun. 2010.

[16] M. Ferrera, Y. Park, L. Razzari, B. E. Little, S. T. Chu, R. Morandotti, D. J. Moss, J. Azaña, "All-optical first and second-order integration on a chip," *Opt. Express*, vol. 19, no. 23, pp. 23153-23161, Oct. 2011.

[17] F. Liu, T. Wang, L. Qiang, T. Ye, Z. Zhang, M. Qiu, and Y. Su, "Compact optical temporal differentiator based on silicon microring resonator," *Opt. Express*, vol. 16, no. 20, pp. 15880–15886, Sep. 2008.

[18] D. Hillerkuss, M. Winter, M. Teschke, A. Marculescu, J. Li, G. Sigurdsson, K. Worms, S. Ben Ezra, N. Narkiss, W. Freude, and J. Leuthold, "Simple all-optical FFT scheme enabling Tbit/s real-time signal processing," *Opt. Express*, vol. 18, no. 9, pp. 9324-9340, Apr. 2010.

[19] D. Hillerkuss, R. Schmogrow, T. Schellinger, M. Jordan, M. Winter, G. Huber, T. Vallaitis, R. Bonk, P. Kleinow, F. Frey, M. Roeger, S. Koenig, A. Ludwig, A. Marculescu, J. Li, M. Hoh, M. Dreschmann, J. Meyer, S. Ben Ezra, N. Narkis, B. Nebendahl,

F. Parmigiani, P. Petropoulos, B. Resan, A. Oehler, K. Weingarten, T. Ellermeyer, J. Lutz, M. Moeller, M. Huebner, J. Becker, C. Koos, W. Freude, and J. Leuthold, "26 Tbit s^{-1} line-rate super-channel transmission utilizing all-optical fast Fourier transform processing," *Nature Photon.*, vol. 5, no. 6, pp. 364–371, May 2011.

[20] F. Li, Y. Park, and J. Azaña, "Complete temporal pulse characterization based on phase reconstruction using optical ultrafast differentiation (PROUD)," *Opt. Express*, vol. 32, no. 22, pp.3364-3366, Nov. 2007.

[21] R. Slavík, L. K. Oxenløwe, M. Galili, H.C.M. Mulvad, Y. Park, J. Azaña, and P. Jeppesen, "Demultiplexing of 320 Gbit/s OTDM data using ultrashort flat-top pulses," *IEEE Photon. Technol. Lett.*, vol. 19, no. 22, pp. 1855-1857, Nov. 2007.

[22] H. Shahoei, P. Dumais, and J. P. Yao, "Continuously tunable photonic fractional Hilbert transformer using a high-contrast Germanium-doped silica-on-silicon microring resonator," *Opt. Lett.*, vol. 39, no. 9, pp. 2778-2781, May 2014.

[23] C. Sima, J. C. Gates, H. L. Rogers, P. L. Mennea, C. Holmes, M. N. Zervas, and P. G. R. Smith, "Phase controlled integrated interferometric single-sideband filter based on planar Bragg gratings implementing photonic Hilbert transform," *Opt. Express*, vol. 38, no. 5, pp. 727-729, Mar. 2013.

[24] Y. Park, J. Azaña, and R. Slavík, "Ultrafast all-optical first- and higher-order differentiators based on interferometers," *Opt. Lett.*, vol. 32, no. 6, pp. 710-712, Mar. 2007.

[25] C. C. Tseng and S. C. Pei, "Design and application of discrete-time fractional Hilbert transformer*," IEEE Trans. Circuits Syst. II, Analog Digital Signal Process.*, vol. 47, no.12, pp.1529–1533, Dec. 2000.

[26] W. Liu, M. Li, R. Guzzon, E. Norberg, L. A. Coldren, and J. Yao, "A photonic integrated fractional Hilbert transformer with continuous tunability," in Optical Fiber Communication Conference, OSA Technical Digest (online) (Optical Society of America, 2014), paper Tu2A.6.

[27] L.-C. Tsai and H.-S. Fang, "Design and implementation of second-order microwave integrators," *Microw. And Opt. Tech. Lett.*, vol. 53, no. 9, pp. 1983-1986, Sep. 2011.

[28] C.-W. Hsue, L.-C. Tsai, and K.-L. Chen, "Implementation of first-order and second-order microwave differentiator," *IEEE Trans. Microw. Theory Tech.*, vol. 52, no. 5, pp. 1443–1447, May 2004.

[29] B. Mathieu, P. Melchior, A. Oustaloup, and C. Ceyral, "Fractional differentiation for edge detection," *Signal Process.*, vol. 83, no. 11, pp. 2421–2432, Nov. 2003.

[30] P. Saeung and P. P. Yupapin, "Generalized analysis of multiple ring resonator filters: Modeling by using graphical approach," *Optik*, vol. 119, no. 10, pp. 465-472, Dec. 2006.

Acknowledgments: This work was sponsored by the Natural Sciences and Engineering Research Council of Canada (NSERC). The authors also acknowledge support from the Nanofabrication Center at UCSB.

Fig. 1. The schematics of the proposed photonic integrated signal processor. (a) The schematic diagram of the photonic integrated signal processor as a unit cell. (b) A schematic representation of the photonic integrated signal processor consisting of three coupled rings and a bypass waveguide. (c) The fabricated on-chip photonic signal processor prototype. The lower image shows the chip wire bonded to a carrier for experimental test.

Fig. 2. Experimental results when the photonic integrated signal processor is configured as a temporal integrator. (a) The configuration of the first-order integrator. (b) The spectral response without injection current to the PM in the working ring resonator. (c) The spectral response of the integrator when the injection current to the PM in the ring is tuned at three different values. (d) The first-order integration of the Gaussian pulse with an integration time of 10.9 ns. The input Gaussian pulse with a temporal width of 54 ps is shown in the inset. (e) The second-order and third-order integration of the Gaussian pulse. (f) The first-order integration of an in-phase doublet pulse, which is shown in the inset. (g) The first-order integration of an out-of-phase doublet pulse.

Fig. 3. Experimental results when the photonic integrated signal processor is configured as a fractional differentiator. (a) The configuration. (b) The spectral response with six different injection currents to the PM in the input tunable coupler of the MZI. (c) The spectral response and (d) phase response of the differentiator when the injection current to the PM in the MZI is tuned at four different values. (e) The input Gaussian pulse with a temporal width of 33 ps. (f) to (j) The fractional differentiation of the input Gaussian pulse with a fraction order of (f) 0.785, (g) 0.842, (h) 1, (i)1.2, and (j) 1.68.

Fig. 4. Experimental results when the photonic integrated signal processor is configured as a Hilbert transformer. (a) The configuration. (b) The spectral response with four different injection currents to the PM in working ring resonator. (c) The spectral response and (d) phase response of the differentiator when the injection current to the PM in the working ring is tuned at four different values. (e) The input Gaussian pulse with a temporal width of 33 ps. (f) to (h) The fractional Hilbert transform of the input Gaussian pulse

with a fraction order of (f) 0.5, (g) 0.725, and (h) 1. (i) and (j) shows the results of the cascaded Hilbert transformers with fraction orders of (1.0, 0.25) and (1.0, 1.0).

Fig. 5. Estimated processing error as a function of the input pulse bandwidth for a (a) temporal integrator, (b) temporal differentiator, and (c) Hilbert transformer.

Fig. 1

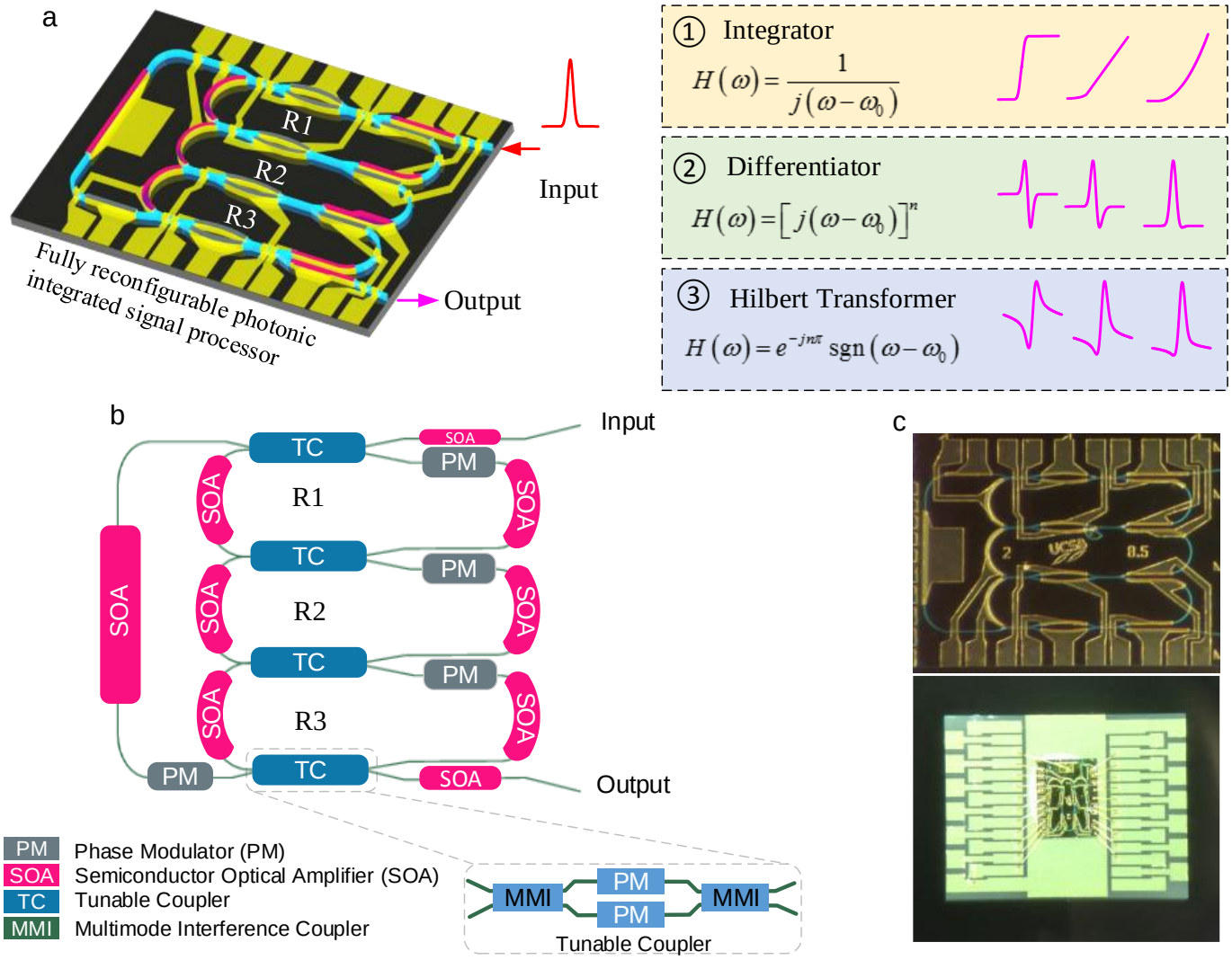
a
R1
R2
R3
Input
Output
Fully reconfigurable photonic integrated signal processor
① Integrator
$H(\omega)=\frac{1}{j(\omega-\omega_0)}$
② Differentiator
$H(\omega)=\left[j(\omega-\omega_0)\right]^n$
③ Hilbert Transformer
$H(\omega)=e^{-jn\pi}\,\mathrm{sgn}(\omega-\omega_0)$
b
Input
Output
TC
SOA
PM
R1
R2
R3
PM Phase Modulator (PM)
SOA Semiconductor Optical Amplifier (SOA)
TC Tunable Coupler
MMI Multimode Interference Coupler
MMI
PM
PM
MMI
Tunable Coupler
c

Fig. 2

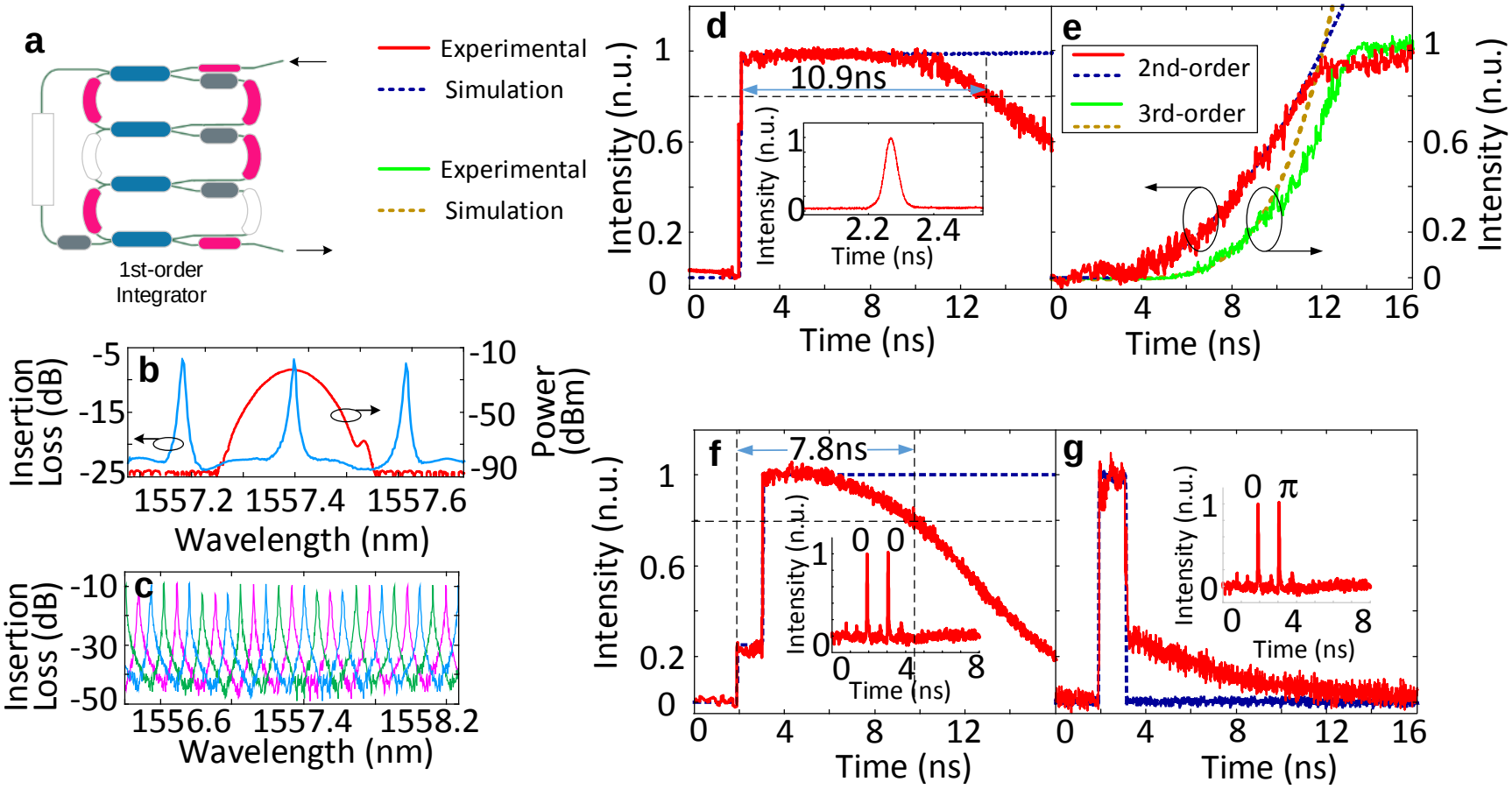
a
1st-order
Integrator
Experimental
Simulation
Experimental
Simulation
b
Insertion Loss (dB)
Power (dBm)
Wavelength (nm)
c
Insertion Loss (dB)
Wavelength (nm)
d
10.9ns
Intensity (n.u.)
Time (ns)
e
2nd-order
3rd-order
Intensity (n.u.)
Time (ns)
f
7.8ns
Intensity (n.u.)
Time (ns)
g
0 π
Intensity (n.u.)
Time (ns)

Fig. 3

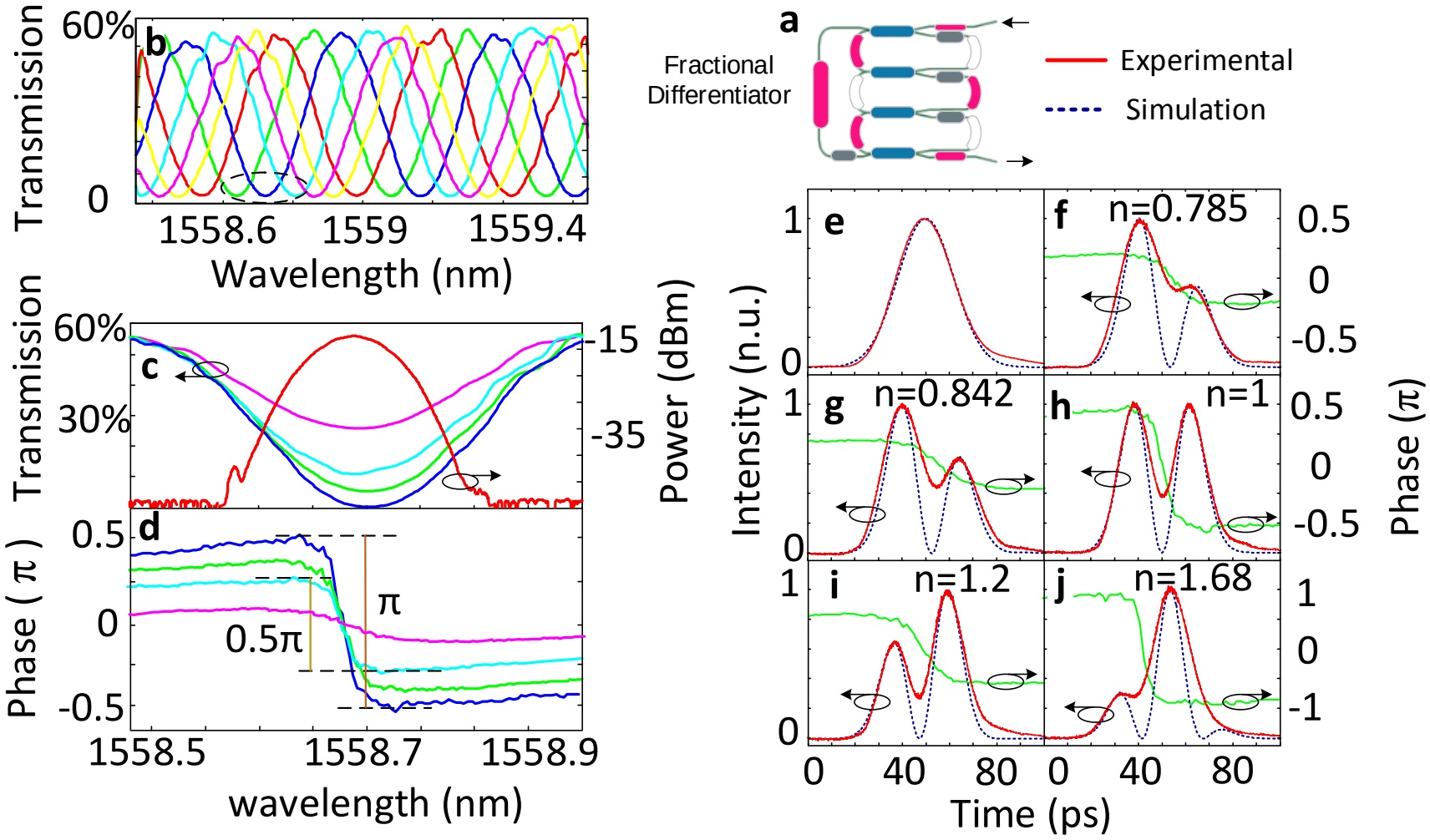
a
Fractional Differentiator
Experimental
Simulation
b
60%
0
Transmission
1558.6
1559
1559.4
Wavelength (nm)
c
60%
30%
Transmission
-15
-35
Power (dBm)
d
0.5
0
-0.5
Phase (π)
π
0.5π
1558.5
1558.7
1558.9
wavelength (nm)
e
f
n=0.785
g
n=0.842
h
n=1
i
n=1.2
j
n=1.68
1
0
Intensity (n.u.)
0.5
0
-0.5
Phase (π)
1
0
-1
0
40
80
Time (ps)

Fig. 4

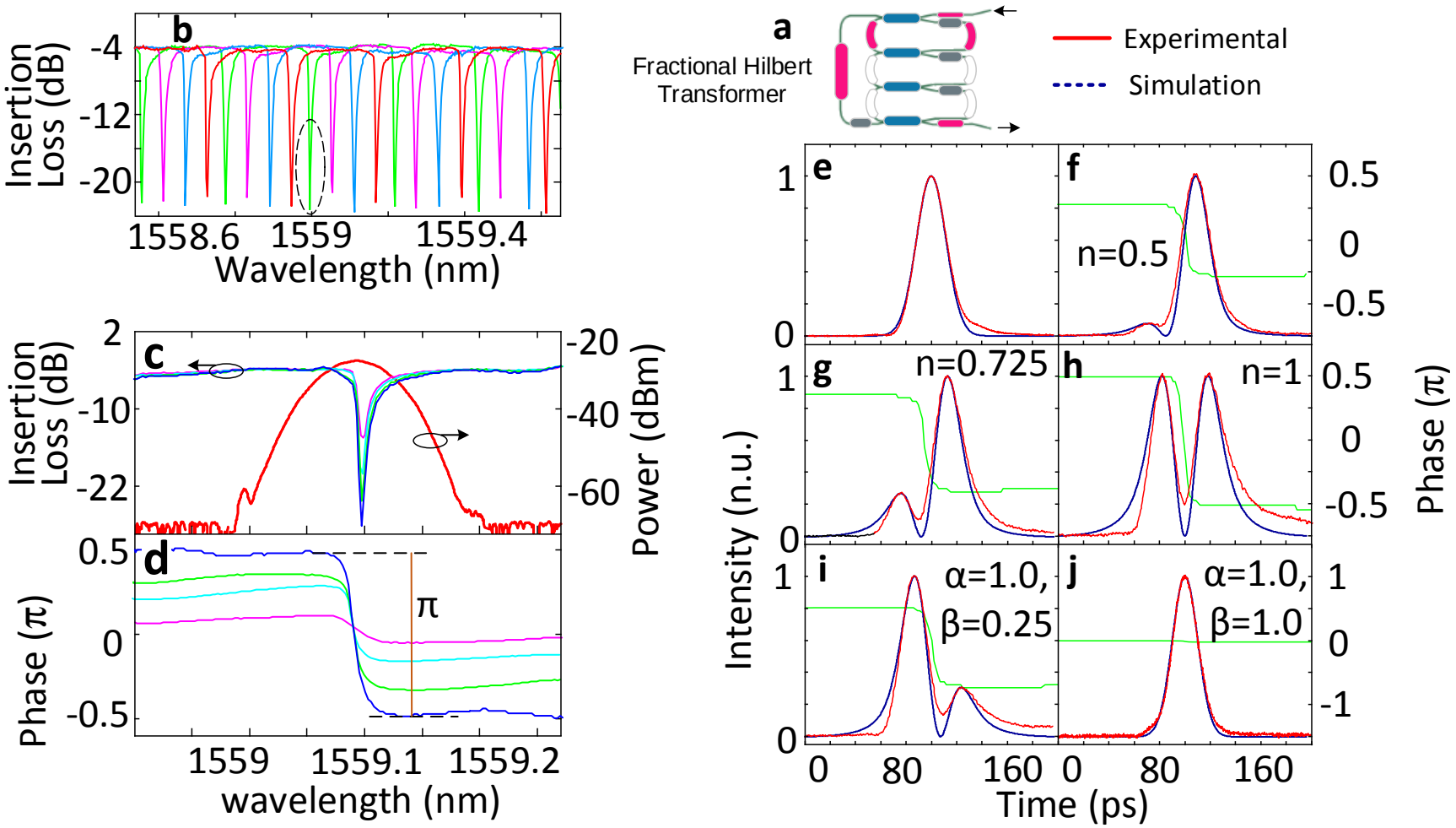
a
Fractional Hilbert Transformer
Experimental
Simulation
b
Insertion Loss (dB)
-4
-12
-20
1558.6
1559
1559.4
Wavelength (nm)
c
d
Insertion Loss (dB)
2
-10
-22
-20
-40
-60
Power (dBm)
Phase (π)
0.5
0
-0.5
π
1559
1559.1
1559.2
wavelength (nm)
e
f
g
h
i
j
n=0.5
n=0.725
n=1
α=1.0,
β=0.25
α=1.0,
β=1.0
Intensity (n.u.)
1
0
0.5
-0.5
-1
0
80
160
Time (ps)
Phase (π)

Fig. 5

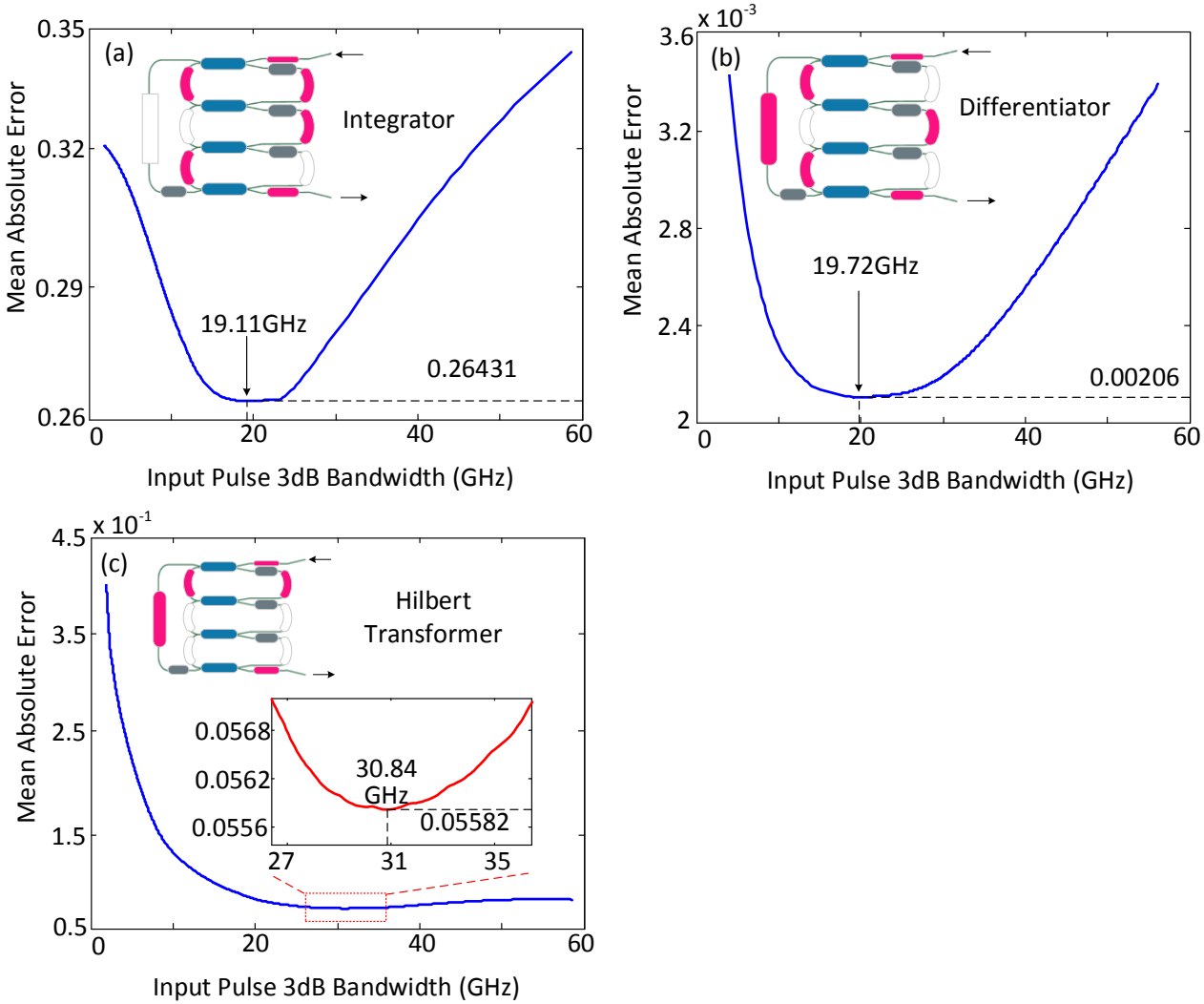
(a)
Integrator
19.11GHz
0.26431
Mean Absolute Error
Input Pulse 3dB Bandwidth (GHz)
0.35
0.32
0.29
0.26
0
20
40
60
(b)
x 10-3
Differentiator
19.72GHz
0.00206
3.6
3.2
2.8
2.4
2
(c)
x 10-1
Hilbert
Transformer
30.84
GHz
0.05582
0.0568
0.0562
0.0556
27
31
35
4.5
3.5
2.5
1.5
0.5

Materials and Methods

Multifunction configuration

The photonic integrated signal processor can be configured as a temporal integrator, a temporal differentiator, and a Hilbert transformer. Fig. M1(a) shows the general configuration of the signal processor which consists of three rings and one bypass waveguide, with nine SOAs and twelve PMs in the rings. Fig. M1(b) shows the signal processor that is reconfigured to have a single, double, and triple coupled rings by shutting off the marked SOAs to achieve a first-, second-, and third-order integrator. The three temporal waveforms are the results of the integration of a Gaussian pulse with three different orders of 1, 2, and 3.

Fig. M1(c) shows the signal processor that is reconfigured to have an MZI structure by shutting off the marked SOAs to achieve a fractional-order temporal differentiator. The operation wavelength can also be tuned by adjusting the injection current to a PM in one arm of the MZI. The four output temporal waveforms are the results of the differentiation of a Gaussian pulse with four different fractional orders of 1, 0.5, 0.25 and 0.05.

Fig. M1(d) shows the signal processor that is reconfigured to have a single ring or two cascaded rings to implement a fractional Hilbert transformer or two cascaded fractional Hilbert transformers, again by shutting off the marked SOAs. The output temporal waveforms are the results of the fractional Hilbert transformation of a Gaussian pulse with four fractional orders of 1, 0.5, 0.25 and 0.05.

For each of the configurations shown in Fig. M1(b), (c) and (d), Mason's formula can be used to derive the transfer function from a signal flow graph (30). For a temporal differentiator with an MZI structure, the derivation can be found in (24). A detailed derivation of the transfer functions can also be found in the supplementary document. By adjusting the parameters in the transfer functions through tuning the gains of the SOAs and the phase shifts of the PMs, the tuning of the order of a temporal integrator, a fractional-order differentiator, or a fractional-order Hilbert transformer can be achieved in a single photonic integrated circuit. The detailed system parameters to implement those functions in the experiment can be found in the supplementary document in Table S-I, Table S-II, and Table S-III.

Fig. M1. The reconfigurable photonic integrated signal processor**.** (a) The general configuration of the signal processor. (b) Reconfigured as a first-, second-, and third-order integrator. (c) Reconfigured as a fractional differentiator. (d) Reconfigured as a single and two cascaded factional Hilbert transformers.

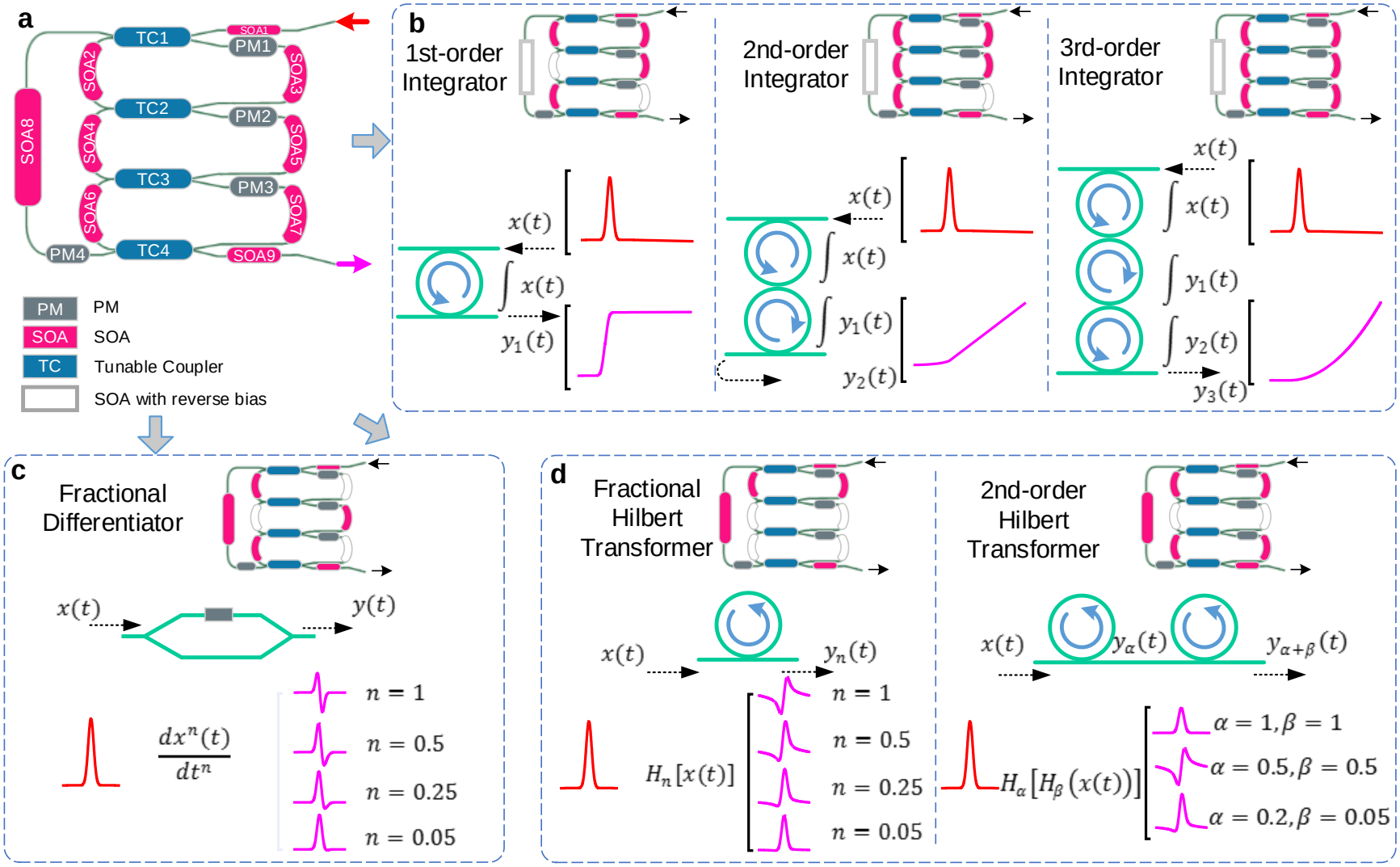
a
TC1
TC2
TC3
TC4
PM1
PM2
PM3
PM4
SOA1
SOA2
SOA3
SOA4
SOA5
SOA6
SOA7
SOA8
SOA9
PM
SOA
TC
Tunable Coupler
SOA with reverse bias
b
1st-order Integrator
2nd-order Integrator
3rd-order Integrator
$x(t)$
$\int x(t)$
$y_1(t)$
$y_2(t)$
$y_3(t)$
c
Fractional Differentiator
$y(t)$
$\frac{dx^n(t)}{dt^n}$
$n = 1$
$n = 0.5$
$n = 0.25$
$n = 0.05$
d
Fractional Hilbert Transformer
2nd-order Hilbert Transformer
$y_n(t)$
$H_n[x(t)]$
$y_\alpha(t)$
$y_{\alpha+\beta}(t)$
$H_\alpha[H_\beta(x(t))]$
$\alpha = 1, \beta = 1$
$\alpha = 0.5, \beta = 0.5$
$\alpha = 0.2, \beta = 0.05$

Device fabrication

The designed chip with a single unit cell has a size of 1.5 mm x 2 mm. In the unit cell, the length of each ring resonator is 3 mm. Two 400-μm SOAs with a confinement tuning layer offset quantum well (CTL-OQW) structure are fabricated in each ring to provide a peak gain of 9.6 dB per SOA to compensate for the insertion loss or to shut off the ring. With the ring length of 3 mm subtracting the length of the two SOAs (400 μm each) in each ring resonator and 7.4 $dBcm^{-1}$ of passive waveguide loss, the total waveguide propagation loss is 1.6 dB for each ring resonator. In addition, each MMI coupler in the ring resonator has 0.5 dB insertion loss. Thus the total round-trip loss is ~3.6 dB, which can be compensated by the SOAs. In the bypass waveguide, there is an SOA with a length of 600 μm to compensate for the insertion loss or to shut off the bypass waveguide. Two additional active SOAs are incorporated into the processor at the input and output waveguides to compensate for the fiber coupling losses, as shown in Fig. 1. In addition, the facets of the bypass waveguides are angled at 7^o to minimize the reflections. The peak power of the input optical signal should be below ~13 dBm to avoid damaging the input/output facets. The phase modulation in the ring and the tuning of the coupler are accomplished by forward bias currents via current injection and free carrier absorption through the carrier plasma effect in the PMs. The PMs in the chip are fabricated with a length of 300 μm.

The chip was fabricated on a quarter of a wafer that was grown at UCSB. At the beginning, the areas in the chip for the SOAs, passive (low loss waveguide propagation), and phase modulator, are defined by using semiconductor wet-etching techniques. After regrowth, the deeply-etched waveguides are defined. The waveguide etch is performed using a 200^oC ICP-RIE dry etch. To make contact to SOAs and PMs, vias need to be constructed and metallization applied to the device. First, the newly-etched sample is coated in 300 nm of silicon nitride using PECVD. This provides the electrical insulation required such that metal traces and pads can be placed on the surface of the photonic integrated chip (PIC). Then, a partial exposure is performed on sections of waveguide where vias are desired.

To ease testing, the chips need to be cleaved apart and made secure on a carrier for wire bonding. The carrier provides structural integrity and large pads for probing with probe cards. The individual devices are mounted with solder onto an aluminum nitride carrier and then wire-bonded to the carrier pads.

Pulse Generation and Measurement

We used a mode-locked laser source with a repetition rate of 48.6 MHz and a central wavelength at 1558.7 nm to generate an optical pulse, and the pulse width is controlled by a programmable optical filter (Finisar, WaveShaper 4000S) connected at the output of the mode-locked laser source. The in-phase and out-of-phase doublet pulses are generated using an unbalanced MZI by launching an optical Gaussian pulse into the MZI with a length difference between the two arms of 25 cm. As a result, two closely separated pulses with a temporal separation of 1.14 ns are generated. Depending on the phase shift applied to one pulse by a phase modulator in one arm of the MZI, an in-phase (no phase shift) or out-of-phase (π phase shift) doublet pulse is generated.

Supplementary Information

1) Power budget

By adjusting the injection currents to the SOAs and PMs, the photonic signal processor can be reconfigured to operate as an integrator, differentiator, and Hilbert transformer. The injection currents and the power consumptions are summarized in Table S-I, Table S-II, and Table S-III.

Table S-I. The injection currents when the processor is configured as an integrator.

Components	**1**st-order Integrator	**2**nd-order Integrator	**3**rd-order Integrator
SOA1	28.806mA	28.806mA	28.806mA
SOA2	20.504mA	20.504mA	20.504mA
SOA3	19.325mA	19.325mA	19.325mA
SOA4	1.005µA	21.412mA	21.412mA
SOA5	24.000mA	19.822mA	19.822mA
SOA6	24.532mA	24.532mA	21.001mA
SOA7	-1.130µA	-1.130µA	22.851mA
SOA8	-10.213µA	-10.213µA	-10.213µA
SOA9	29.006mA	29.006mA	29.006mA
PM1	0	0	0
PM2	0	1.290mA	1.290mA
PM3	0	0	0.752mA
PM4	0	0	0
TC1	1.950mA	1.950mA	1.950mA
TC2	1.942mA	1.942mA	1.942mA
TC3	0	1.833mA	1.833mA
TC4	0	0	1.906mA
Power	350.475mW	381.851mW	419.695mW

Table S-II. The injection currents when the processor is configured as a differentiator.

Components	Fractional Differentiator n=0.785	Fractional Differentiator n=0.842	Fractional Differentiator n=1.000	Fractional Differentiator n=1.200	Fractional Differentiator n=1.680
SOA1	28.806mA	28.806mA	28.806mA	28.806mA	28.806mA
SOA2	25.131mA	25.131mA	25.131mA	25.131mA	25.131mA
SOA3	-1.005µA	-1.005µA	-1.005µA	-1.005µA	-1.005µA
SOA4	-1.133µA	-1.133µA	-1.133µA	-1.133µA	-1.133µA
SOA5	24.000mA	24.000mA	24.000mA	24.000mA	24.000mA
SOA6	24.532mA	24.532mA	24.532mA	24.532mA	24.532mA
SOA7	-1.142µA	-1.142µA	-1.142µA	-1.142µA	-1.142µA
SOA8	33.617mA	33.617mA	33.617mA	33.617mA	33.617mA
SOA9	29.006mA	29.006mA	29.006mA	29.006mA	29.006mA
PM1	0	0	0	0	0
PM2	0	0	0	0	0
PM3	0	0	0	0	0
PM4	0	0	0	0	0
TC1	1.051mA	1.051mA	1.051mA	1.051mA	1.051mA
TC2	0	0	0	0	0
TC3	0	0	0	0	0
TC4	0.276mA	0.535mA	1.028mA	1.505mA	1.811mA
Power	419.296mW	419.650	420.201mW	421.604mW	422.126mW

Table S-III. The injection currents when the processor is configured as a Hilbert transformer.

Components	Fractional Hilbert Transformer n=0.500	Fractional Hilbert Transformer n=0.725	Fractional Hilbert Transformer n=1.000	Hilbert Transformer α=1.000, β=0.250	Hilbert Transformer α=1.000, β=1.000
SOA1	28.806mA	28.806mA	28.806mA	28.806mA	28.806mA
SOA2	20.504mA	20.504mA	20.504mA	20.504mA	20.504mA
SOA3	19.519mA	19.519mA	19.519mA	19.519mA	19.519mA
SOA4	-0.002 μA	-0.006 μA	-0.007 μA	-0.007 μA	-0.007 μA
SOA5	-0.004 μA	-0.018 μA	-0.113 μA	-0.113 μA	-0.113 μA
SOA6	-0.006 μA	-0.006 μA	-0.008μA	21.001mA	21.001mA
SOA7	-0.015 μA	-0.023 μA	-0.051 μA	22.851mA	22.851mA
SOA8	33.617mA	33.617mA	33.617mA	33.617mA	33.617mA
SOA9	29.006mA	29.006mA	29.006mA	29.006mA	29.006mA
PM1	0	0	0	0	0
PM2	0	0	0	0	0
PM3	0	0	0	0.752mA	1.025V/0.752mA
PM4	0	0	0	0	0
TC1	0.539mA	0.871mA	1.051mA	1.051mA	1.051mA
TC2	2.390mA	2.390mA	2.390mA	2.390mA	2.390mA
TC3	0	0	0	2.173mA	2.173mA
TC4	2.337mA	1.836V/2.337mA	2.337mA	0.273mA	2.437mA
Power	324.935mW	325.385mW	325.652mW	418.919mW	423.79mW

2) Application examples using the photonic integrated signal processor

I. Image processing

Image processing such as edge enhancement by differentiation can be implemented by the proposed photonic signal processor. For example, an image can be encoded in a temporally stretched optical pulse based on wavelength to space mapping [1], which can be processed by the proposed photonic signal processor. To demonstrate the image enhancement concept, here we use five temporal waveforms to emulate five analog image signals, as shown in Fig. S1(a), (b), (c), (d) and (e). The differentiations of the five waveforms by the proposed photonic signal processor are shown in Fig. S1(f), (g),(h), (i) and (j). As can be seen, the transitions (corresponding to the edges in an image) in a square, a sawtooth, a triangular, a trapezoidal, and a stepped waveform are enhanced. The experimental results are also consistent with the simulation results as shown in Fig. S1(k), (l), (m), (n), and (o).

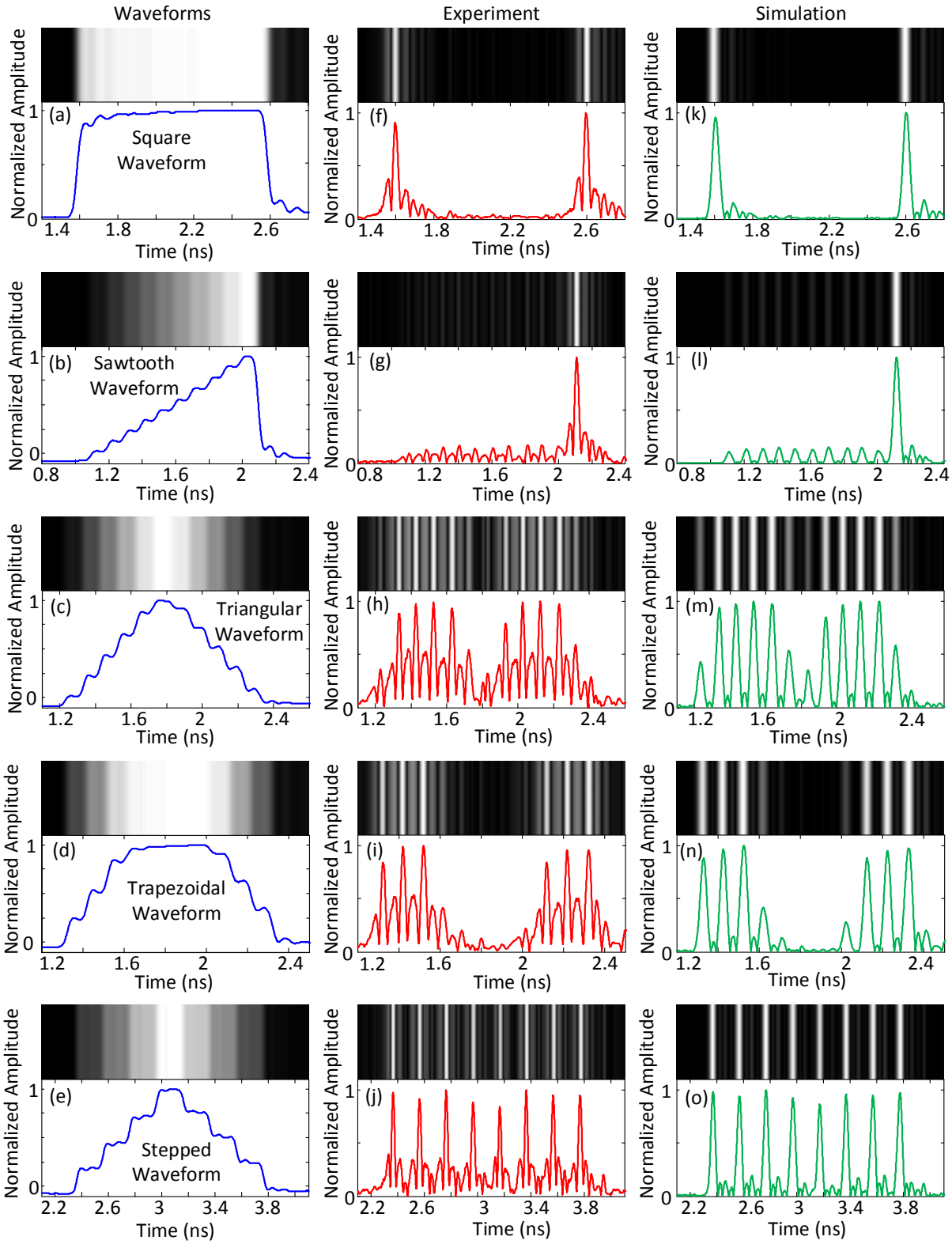

Fig. S1. Experimental results (red) to show the transition enhancement by the proposed photonic signal processor. Simulation results (green) are also shown for comparison. Transitions in a (a) square, (b) sawtooth, (c) triangular, (d) trapezoidal, and (e) stepped waveform, are enhanced by the proposed photonic signal processor as shown in (f), (g), (h), (i), and (j). The simulation results are shown in (k), (l), (m), (n), and (o) for comparison.

II. Hilbert transform for SSB modulation

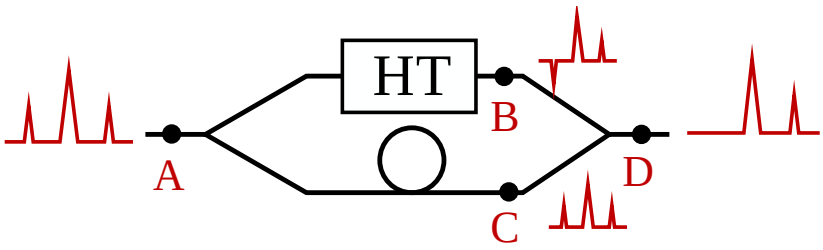

Fig. S2. Experimental setup for the demonstration of SSB modulation using the proposed signal processor reconfigured as a Hilbert transformer. HT: Hilbert transformer.

To achieve SSB modulation, the proposed photonic signal processor is reconfigured as a Hilbert transformer, which is incorporated in a Mach-Zehnder interferometer (MZI), as shown in Fig. S2. A double-sideband (DSB) modulated optical signal is sent into the MZI. A Hilbert transformer can provide a π phase shift to one sideband of the DSB modulated optical signal, thus the combination of two DSB modulated signals at the output of the MZI will cancel one sideband, and an SSB modulated optical signal is thus obtained. The spectrum of the generated SSB modulated optical signal is measured by an optical spectra analyzer (OSA), which is shown in Fig. S3.

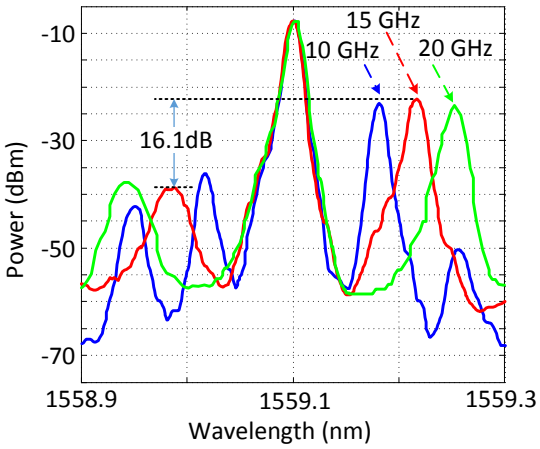

Fig. S3. The spectrum of the experimentally generated SSB modulated optical signal.

As can be seen from Fig. S3, an optical SSB-modulated optical signal is generated. The sideband suppression ratio is 12.7 dB, 16.1 dB, and 13.8 dB when the frequency of the modulation signal is 10 GHz, 15 GHz, and 20 GHz, respectively.

3) The transfer functions of the proposed photonic signal processor reconfigured as an integrator, Hilbert transformer, and differentiator.

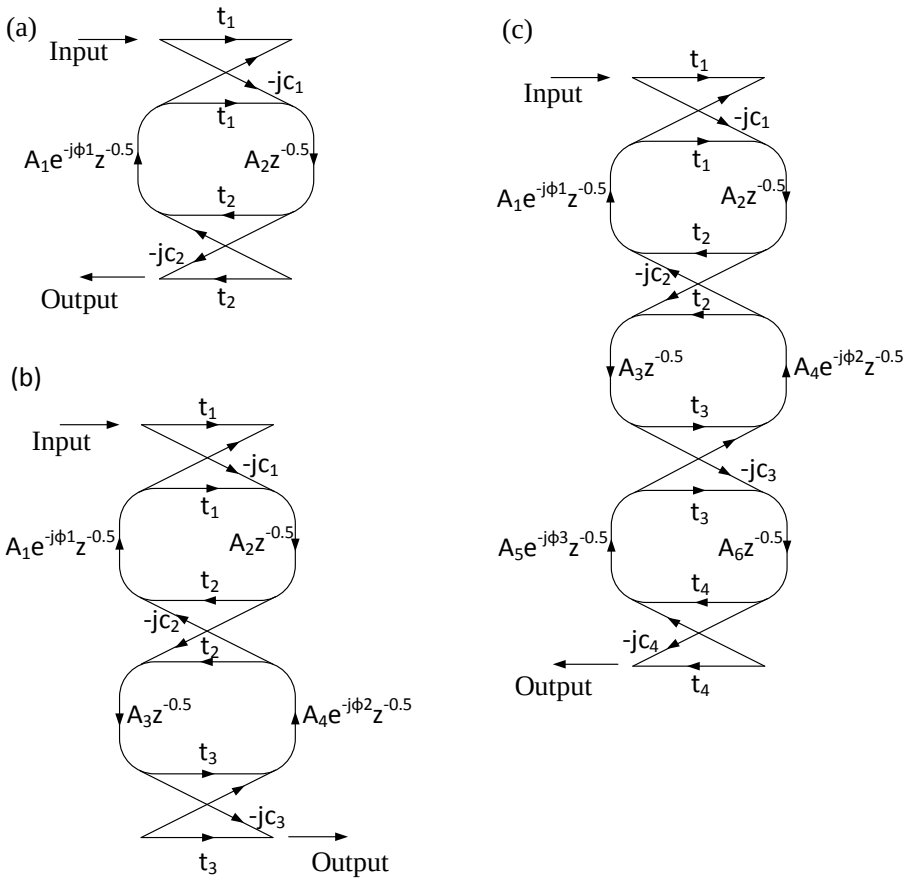

Fig. S4. Signal flow graphs of (a) single add/drop ring, (b) two coupled rings, and (c) three coupled rings.

I. First order integrator

A first order integrator can be implemented using a single add/drop ring resonator in the proposed signal processor, as shown in Fig. S4(a). The transfer function is given by [2]

$$H_1(z) = -\frac{c_1 c_2 A_2 z^{-1/2}}{1 - t_1 t_2 A_1 A_2 z^{-1}} = \frac{c_1 c_2 A_2 e^{-\frac{1}{2} j\omega\tau}}{1 - t_1 t_2 A_1 A_2 e^{-j\omega\tau}} = \frac{c_1 c_2 A_2}{e^{\frac{1}{2} j\omega\tau} - t_1 t_2 A_1 A_2 e^{-\frac{1}{2} j\omega\tau}} \tag{S-1}$$

where $z^{-1} = e^{-j\omega\tau}$, ω is the angular frequency, $\omega_0 = 2m\pi/\tau$ is the frequency of interests in one of the resonance frequencies, m is an arbitrary integer, $\tau = n_{eff} L/c$ is a time constant, n_{eff} is the effective refractive index of the waveguide, L is the length of the ring resonator, c_i is the amplitude coupling value of the i^{th} coupler, $t_i = \sqrt{1 - c_i^2}$ assuming that there is no coupler insertion loss, φ_i is the phase introduced by the phase modulator in the i^{th} ring, and A_i is the fractional amplitude loss in each waveguide segment.

By tuning the gain in the ring resonator to make $t_1 t_2 A_1 A_2 \approx 1$ and assuming m=0, we have

$$H_1(\omega)=\frac{c_1c_2A_2}{e^{\frac{1}{2}j\omega\tau}-e^{-\frac{1}{2}j\omega\tau}}=\frac{c_1c_2A_2}{2j\sin\left[\frac{1}{2}(\omega-\omega_0)\tau+m\pi\right]}\approx\frac{c_1c_2A_2/\tau}{j(\omega-\omega_0)} \tag{S-2}$$

As can be seen that a single add/drop ring resonator with a transfer function of (S-2) can be used to implement a first order integrator.

II. Second order integrator

A second order integrator can be implemented using two coupled add/drop ring resonators in the proposed signal processor, as shown in Fig. S4(b). The transfer function is given by [2]

$$H_2(z)=\frac{jc_1c_2c_3A_2A_3z^{-1}}{1-B_1z^{-1}+B_2z^{-2}}=\frac{jc_1c_2c_3A_2A_3e^{-j\omega\tau}}{1-B_1e^{-j\omega\tau}+B_2e^{-2j\omega\tau}} \tag{S-3}$$

where

$$B_1=t_1t_2A_1A_2e^{-j\varphi_1}+t_2t_3A_3A_4e^{-j\varphi_2} \tag{S-4}$$

$$B_2=t_1t_3A_1A_2A_3A_4e^{-j(\varphi_1+\varphi_2)} \tag{S-5}$$

If we tune the two coupled rings to have the same resonance frequency, we have $\varphi_1=\varphi_2$. By tuning the gain coupling in each ring resonator we can also have (S-3) written as

$$H_2(\omega)=\frac{jc_1c_2c_3A_2A_3}{\left[e^{-\frac{1}{2}j\omega\tau}-e^{\frac{1}{2}j\omega\tau}\right]^2}=\frac{jc_1c_2c_3A_2A_3}{\left\{2j\sin\left[\frac{1}{2}(\omega-\omega_0)\tau+m\pi\right]\right\}^2}\approx\frac{jc_1c_2c_3A_2A_3/\tau^2}{\left[j(\omega-\omega_0)\right]^2} \tag{S-6}$$

As can be seen that two coupled add/drop ring resonators with a transfer function of (S-6) can be used to implement a second order integrator.

III. Third order integrator.

A third order integrator can be implemented using three coupled add/drop ring resonators in the proposed signal processor, as shown in Fig. S4(c). The transfer function is given by [2],

$$H_3(z)=\frac{c_1c_2c_3c_4A_2A_3A_6z^{-3/2}}{1-D_1z^{-1}+D_2z^{-2}+D_3z^{-3}} \tag{S-7}$$

where

$$D_1=t_1t_2A_1A_2e^{-j\varphi_1}+t_2t_3A_3A_4e^{-j\varphi_2}+t_3t_4A_5A_6e^{-j\varphi_3} \tag{S-8}$$

$$D_2 = t_1 t_3 A_1 A_2 A_3 A_4 e^{-j(\varphi_1+\varphi_2)} + t_2 t_4 A_3 A_4 A_5 A_6 e^{-j(\varphi_2+\varphi_3)} + t_1 t_2 t_3 t_4 A_1 A_2 A_5 A_6 e^{-j(\varphi_1+\varphi_3)} \quad \text{(S-9)}$$

$$D_3 = -t_1 t_4 A_1 A_2 A_3 A_4 A_5 A_6 e^{-j(\varphi_1+\varphi_2+\varphi_3)} \quad \text{(S-10)}$$

Similarly, by tuning the gain and coupling we can rewrite (S-7) as

$$H_3(\omega) \approx \frac{c_1 c_2 c_3 c_4 A_2 A_3 A_6 / \tau^3}{\left[j(\omega - \omega_0) \right]^3} \quad \text{(S-11)}$$

As can be seen that three coupled add/drop ring resonators with a transfer function of (S-11) can be used to implement a third order integrator.

IV. Fractional Hilbert transformer

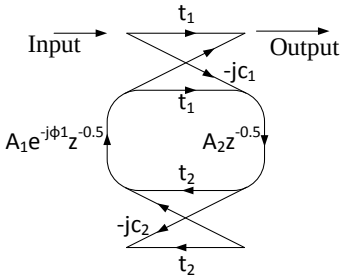

Fig. S5. Signal flow graphs of a single ring.

A fractional Hilbert transformer can be implemented using a single ring resonator, as shown in Fig. S5. The transfer function is given by [2],

$$H_{1t}(z) = \frac{t_1 - t_2 A_1 A_2 z^{-1}}{1 - t_1 t_2 A_1 A_2 z^{-1}} = \frac{t_1 - t_2 A_1 A_2 e^{-j\omega\tau}}{1 - t_1 t_2 A_1 A_2 e^{-j\omega\tau}} \quad \text{(S-12)}$$

Since the loss in the ring resonator can be compensated by the gain provided by the SOAs, $t_2 A_1 A_2$ is close to unity, thus we have (S-12) rewritten as

$$H_{1t}(\omega) \approx \frac{t_1 - e^{-j\omega\tau}}{1 - t_1 e^{-j\omega\tau}} = -\frac{e^{-\frac{1}{2}j\omega\tau} - t_1 e^{\frac{1}{2}j\omega\tau}}{e^{\frac{1}{2}j\omega\tau} - t_1 e^{-\frac{1}{2}j\omega\tau}} = \left| H_{1t}(\omega) \right| e^{j\Psi(\omega)} \quad \text{(S-13)}$$

As can be seen from (S-13), the numerator, $e^{-\frac{1}{2}j\omega\tau} - t_1 e^{\frac{1}{2}j\omega\tau}$, in the transfer function is the complex conjugate of the denominator, $e^{\frac{1}{2}j\omega\tau} - t_1 e^{-\frac{1}{2}j\omega\tau}$. Therefore, its magnitude response can be given as

$$\left|H_{1t}\left(\omega\right)\right|=1 \tag{S-14}$$

and its phase response is written as

$$\begin{aligned}\Psi\left(\omega\right)&=\pi+2\tan^{-1}\frac{\left(1+t_1\right)\sin\frac{1}{2}\omega\tau}{\left(1-t_1\right)\cos\frac{1}{2}\omega\tau}\\&=\pi+2\tan^{-1}\frac{\left(1+t_1\right)\sin\frac{\omega}{\omega_0}m\pi}{\left(1-t_1\right)\cos\frac{\omega}{\omega_0}m\pi}\end{aligned} \tag{S-15}$$

For simplicity, we set *m*=1, and we rewrite (S-15) as

$$\Psi\left(\omega\right)=\pi+2\tan^{-1}\frac{\left(1+t_1\right)\sin\frac{\omega}{\omega_0}\pi}{\left(1-t_1\right)\cos\frac{\omega}{\omega_0}\pi} \tag{S-16}$$

When $\omega\approx\omega_0$ with $\omega<\omega_0$, we have

$$\tan^{-1}\frac{\left(1+t_1\right)\sin\frac{\omega}{\omega_0}\pi}{\left(1-t_1\right)\cos\frac{\omega}{\omega_0}\pi}<0 \tag{S-17}$$

When $\omega\approx\omega_0$ with $\omega>\omega_0$, we have

$$\tan^{-1}\frac{\left(1+t_1\right)\sin\frac{\omega}{\omega_0}\pi}{\left(1-t_1\right)\cos\frac{\omega}{\omega_0}\pi}>0 \tag{S-18}$$

As can be seen from (S-16), (S-17), and (S-18), there is a phase change at frequency $\omega=\omega_0$, and the phase change amount can be controlled by t_1. Therefore, the through ring resonator can be used to implement a fractional Hilbert transformer (Eq. 3 in the manuscript). By varying the coupling coefficient t_1, different values of the fractional order are achieved.

V. Differentiator

A fractional differentiator can be implemented using an MZI. Assuming that τ is the relative time delay between the two MZI arms, the transfer function can be written as [3]

$$H(z)=1+z^{-1}=1+e^{-j\omega\tau} \tag{S-19}$$

where $z^{-1}=e^{-j\omega\tau}$. By setting the interferometer to operate at a minimum transmission at the frequency of interest ($H(\omega_0)=0$), we have

$$\tau=\frac{(2m+1)\pi}{\omega_0} \tag{S-20}$$

where *m* is an arbitrary integer. (S-19) can then be rewritten as

$$\begin{aligned} H(\omega-\omega_0)&=1+e^{-j\omega\tau}=1+e^{-j(\omega-\omega_0)\tau}e^{j\omega_0\tau}=1-e^{-j(\omega-\omega_0)\frac{(2m+1)\pi}{\omega_0}} \\ &=1-e^{-j(2m+1)\pi\frac{\omega-\omega_0}{\omega_0}}=1-\cos\left[(2m+1)\pi\frac{\omega-\omega_0}{\omega_0}\right]+j\sin\left[(2m+1)\pi\frac{\omega-\omega_0}{\omega_0}\right] \end{aligned} \tag{S-21}$$

The above function can be approximated over a sufficiently narrow bandwidth $\Delta\omega$ centered at $\omega=\omega_0$ to the following ($\frac{\omega}{\omega_0}\approx 1$, $\sin\left[(2m+1)\pi\frac{\omega-\omega_0}{\omega_0}\right]\approx(2m+1)\pi\frac{\omega-\omega_0}{\omega_0}$, and $\cos\left[(2m+1)\pi\frac{\omega-\omega_0}{\omega_0}\right]\approx 1$.)

$$H(\omega-\omega_0)\approx j\frac{(2m+1)\pi}{\omega_0}(\omega-\omega_0)=j\tau(\omega-\omega_0) \tag{S-22}$$

As can be seen an MZI with a transfer function of (S-22) can be used to implement a differentiator.

4) Optical filter with a flat top and a tunable passband and center frequency

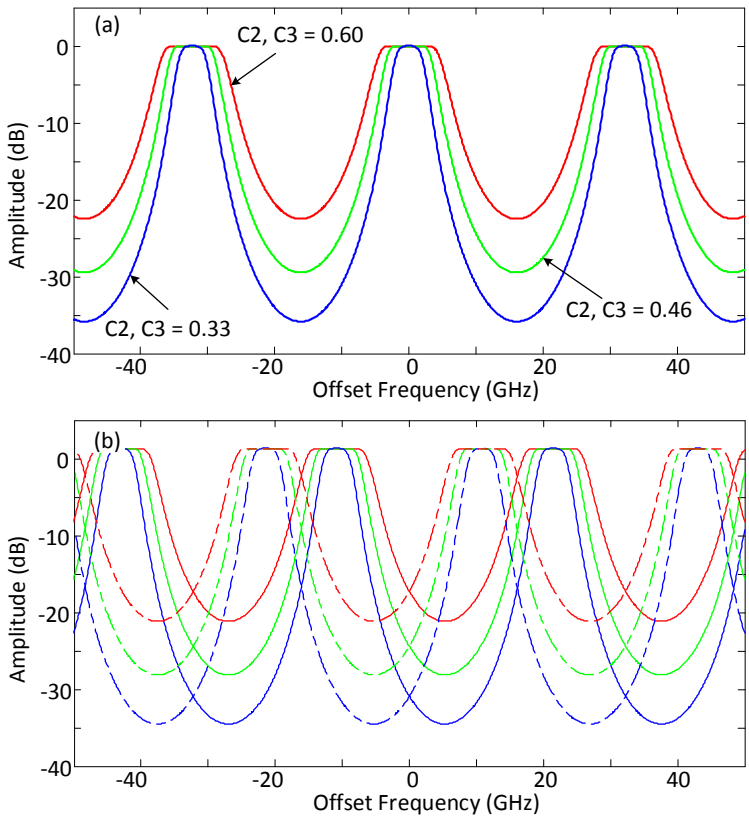

Fig. S6. Three coupled rings for implementing a tunable DWDM filter and the simulation results. (a) The structure. (b) Continuously tunable 3-dB bandwidth from 5 to 10 GHz for a passband with a minimum extinction ratio of 22 dB by adjusting the coupling coefficients C2 and C3. (c) Continuously tunable center frequency of a bandpass by adjusting the phase terms (dashed line, $\phi1= \phi2= \phi3= \phi4=2\pi/3$; solid line, $\phi1= \phi2= \phi3= \phi4=4\pi/3$) via the controlling the injection currents to the PMs in the ring resonators.

The proposed photonic signal processor can also be reconfigured to operate as an optical filter with a flat top and a tunable passband and center frequency. The tunability is achieved by adjusting the currents applied to the active components including the SOAs and PMs in the processor. For example, to implement a tunable DWDM filter, the signal processor can be reconfigured to have a structure with three coupled rings, as shown in Fig. S4(c). A simulation based on the three-coupled-ring structure is implemented [4]. As shown in Fig. S6(a), the filter has a flat top which is achieved by tuning the gain/loss in each of the ring resonators, A1, A2, A3, A4, A5, and A6, and the width of a passband of the DWDM filter is continuously tunable from 5 to 10 GHz by adjusting the coupling coefficients C2 and C3, as indicated in Fig. S4(c). The center frequency of a bandpass is also continuously tunable by adjusting the phase changes in the ring resonators, which are $\phi1$, $\phi2$, $\phi3$, and $\phi4$ as indicated in Fig. S4(c). For example, the center frequency of a bandpass can be shifted by ~10.5 GHz or ~21 GHz if $\phi1=\phi2=\phi3= \phi4=2\pi/3$ or $\phi1=\phi2=\phi3= \phi4=4\pi/3$, as shown in Fig. S6(b). Comparing with a thin film DWDM filter [5], the DWDM filter implemented by the proposed photonic signal processor offers both continuously tunable bandwidth and center frequency. Since the adjacent channel spacing of the implemented DWDM filter is determined by the FSR of the ring resonators, the lengths of the ring resonators

have to be selected to have an FSR corresponding to the wavelength spacing specified by the ITU grid.

References:

[1] K. Goda, K. K. Tsia, and B. Jalali, "Serial time-encoded amplified imaging for real-time observation of fast dynamic phenomena," *Nature*, no. 458, vol. 7242, 1145–1149, Apr. 2009.
[2] P. Saeung and P. P. Yupapin, "Generalized analysis of multiple ring resonator filters: Modeling by using graphical approach," *Optik*, vol. 119, no. 10, pp. 465-472, Dec. 2006.
[3] Y. Park, J. Azaña, and R. Slavík, "Ultrafast all-optical first- and higher-order differentiators based on interferometers," *Opt. Lett.*, vol. 32, no. 6, pp. 710-712, Mar. 2007.
[4] C. Madsen, and J. Zhao, *Optical Filter Design and Analysis: A Signal Processing Approach*, Ch. 5. (Wiley, New York, 1999).
[5] R. Parmentier and M. Lequime, "Substrate-strain-induced tunability of dense wavelength-division multiplexing thin-film filters," *Opt. Lett.*, vol. 28, no. 9, pp. 728-730, May 2003.